

# Discovering New Interactions at Colliders

Kingman Cheung<sup>1</sup> and Robert M. Harris<sup>2</sup>

<sup>1</sup>University of Texas, Austin, TX 78712

<sup>2</sup>Fermilab, Batavia, IL 60510

## ABSTRACT

We summarize results of the 1996 Snowmass workshop on future prospects for discovering dynamical electroweak symmetry breaking, compositeness, and anomalous couplings of quarks at colliders. We present the mass reach of the Tevatron to a color singlet or octet technirho, and to a topgluon or topcolor  $Z'$  from topcolor assisted technicolor. We explore the sensitivity of the Tevatron, LHC, NLC, and VLHC to contact interactions and excited fermions. Finally we investigate the possibility of seeing anomalous couplings of quarks at the Tevatron and LHC.

## I. DYNAMICAL ELECTROWEAK SYMMETRY BREAKING

The mechanism of electroweak symmetry breaking is unknown. The possibility exists that electroweak symmetry is not broken by a fundamental higgs boson, but instead is broken through the dynamics of a new interaction. We explore the discovery potential of future accelerators, and luminosity upgrades to the Tevatron, for two models of dynamical electroweak symmetry breaking: one-family technicolor and topcolor assisted technicolor.

### A. One-Family Technicolor

Eichten and Lane [1] have presented a one-family technicolor model with color triplet techniquarks and color singlet technileptons. The techniquarks will bind to form color singlet technirhos,  $\rho_{T1}^\pm$  and  $\rho_{T1}^0$ , with mass roughly in the range 200 to 400 GeV. Color singlet technirhos are produced in hadron collisions through quark-antiquark annihilation. The expected decay modes are  $\rho_{T1}^\pm \rightarrow W^\pm Z$ ,  $W^\pm \pi_T^0$ ,  $Z \pi_T^\pm$ ,  $\pi_T^\pm \pi_T^0$ , and  $\rho_{T1}^0 \rightarrow W^\pm W^\mp$ ,  $W^\pm \pi_T^\mp$ ,  $\pi_T^\pm \pi_T^\mp$ . Here the technipions,  $\pi_T$ , decay predominantly to heavy flavors:  $\pi_T^0 \rightarrow b\bar{b}$ , and  $\pi_T^\pm \rightarrow c\bar{b}$ ,  $t\bar{b}$ . Techniquarks will also bind to form color octet technirhos,  $\rho_{T8}^0$ , with mass roughly in the range 200 to 600 GeV. Color octet technirhos are produced and decay via strong interactions. If the mass of the colored technipions is greater than half the mass of the technirho, then the color octet technirho will decay predominantly to dijets:  $\rho_{T8} \rightarrow gg$ . If colored technipions are light the color octet technirho decays to pairs of either color triplet technipions (leptoquarks) or color octet technipions.

#### 1. $\rho_{T1} \rightarrow W + \text{dijet at the Tevatron}$

The search for  $\rho_{T1} \rightarrow WX$ , where  $X$  can be a  $W, Z$ , or  $\pi_T$ , is sufficiently similar to the search for a massive  $W'$  decaying to  $WZ$ , that Toback [2] has extrapolated the  $W'$  search to higher luminosities as an estimate of our sensitivity to color singlet technirhos at the Tevatron. He considered the decay chain  $\rho_T \rightarrow WX \rightarrow e\nu + \text{dijets}$ , and required both the electron and

neutrino to have more than 30 GeV of transverse energy,  $E_T$ . He required at least two jets in the event, one with  $E_T > 50$  GeV, and the other with  $E_T > 20$  GeV. The higher  $E_T$  cut on the two jets was optimized for a high mass  $W'$  search ( $M > 500$  GeV) and should be reduced for a lower mass technirho search. The resulting  $W + \text{dijet}$  mass distribution from 110 pb<sup>-1</sup> of CDF data was in good agreement with standard model predictions, and was used to determine the 95% CL upper limit on the  $\rho_{T1}$  cross section, shown in Fig. 1. Here he assumed that the acceptance for a technirho was roughly the same as for a  $W'$ . The extrapolation to higher luminosities shows that TeV33 (30 fb<sup>-1</sup>) should be able to exclude at 95% CL a color singlet technirho decaying to  $W$  plus dijets for technirho masses up to roughly 400 GeV. This covers the expected range in the one-family technicolor model.

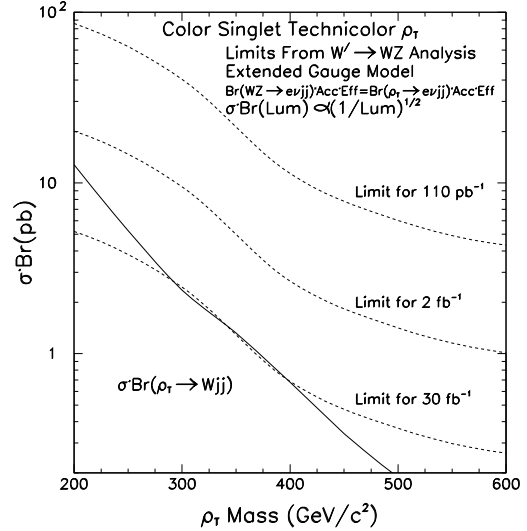


Figure 1: 95% CL upper limit of  $\sigma \cdot Br(\rho_{T1} \rightarrow Wjj)$  vs.  $M_{\rho_T}$ . The solid line is the theoretically expected  $\sigma \cdot Br$  and assumes  $\rho_{T1} \rightarrow WX \rightarrow Wjj = 100\%$ . The dashed lines show predicted limits for 110pb<sup>-1</sup>, 2fb<sup>-1</sup> and 30fb<sup>-1</sup> respectively. Note that we have assumed that the limits simply scale as the inverse of the square root of the luminosity

#### 2. $\rho_{T1} \rightarrow W + b\bar{b}$ at the Tevatron and LHC

Womersley [3] has studied the process  $q\bar{q}' \rightarrow \rho_{T1} \rightarrow W\pi_T \rightarrow (l\nu)(b\bar{b})$ , including the effect of tagging events with a final state  $b$  quark, for the particular case of  $m_{\rho_T} = 210$  GeV and  $m_{\pi_T} = 115$  GeV. He generates signal and background events using ISAJET, and uses a fast simulation of the CMS detector at the LHC. After all simulation, events are required to have a good  $W$  candidate, formed from an isolated charged lepton with  $E_T > 25$  GeV and pseudorapidity  $|\eta| < 1.1$ , a neutrino

with  $E_T > 25$  GeV, and their combined transverse mass in the range  $50 < m_T < 100$  GeV. Further, events were required to have two jets with  $E_T > 20$  GeV and  $|\eta| < 2.5$ , and the probability of tagging at least one of the two b quarks was assumed to be 50% with a mistag rate of 1% for light quarks. Figure 2 show the reconstructed  $\pi_T$  peak in the signal sample, and that prior to b-tagging the signal is swamped by a large QCD W+dijet background. Figure 2 also shows that after b-tagging the signal to background is significantly improved at both the Tevatron and the LHC. For this particular case of a light technirho the signal to background is better at the Tevatron although the rate at the LHC is considerably higher. Clearly, b-tagging is critical, and makes possible the discovery of a 210 GeV color singlet technirho at the Tevatron in Run II ( $2 \text{ fb}^{-1}$ ).

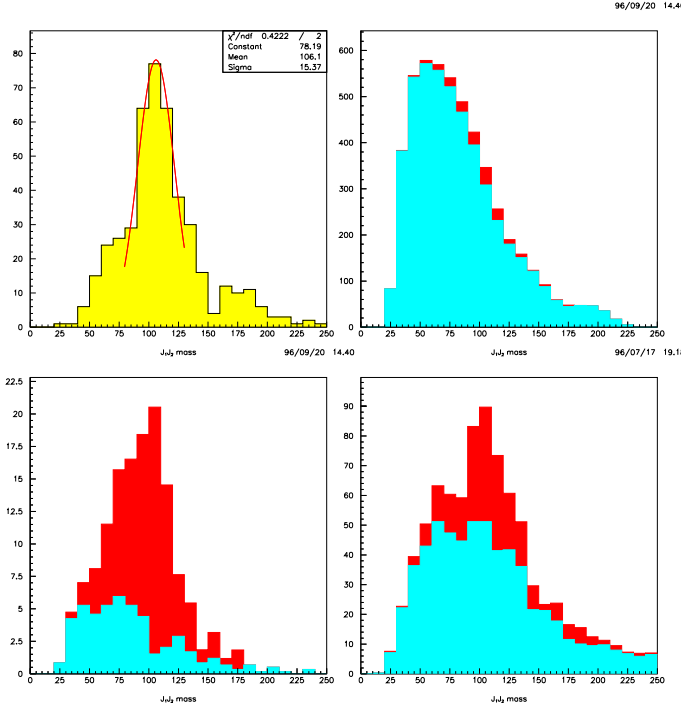


Figure 2:  $\rho_{T1} \rightarrow W + \pi_T \rightarrow (l\nu)(b\bar{b})$  search. (upper left) Leading dijet invariant mass distribution for signal at the LHC. (upper right) Same for signal (dark) and background (light) at the Tevatron before b-tagging. Vertical scale is events/10 GeV/ $2 \text{ fb}^{-1}$ . (lower left) Same at the Tevatron after b-tagging. (lower right) Same at the LHC after b-tagging. Vertical scale is events/10 GeV/ $0.5 \text{ fb}^{-1}$ . All horizontal scales are in GeV.

### 3. $\rho_{T8} \rightarrow$ dijets at the Tevatron

Harris has determined the sensitivity at the Tevatron to dijet decays of color octet technirhos by extrapolating CDF searches [4] to higher luminosities. Here there are significant QCD backgrounds, so the cross section limits scale inversely as the square root of the luminosity. In reference [5] he compared the cross section limit to the theoretical prediction, to determine the mass excluded at 95% CL, shown in fig. 3. The mass reach for color octet technirhos is 0.77 TeV for Run II ( $2 \text{ fb}^{-1}$ ) and 0.90 TeV for TeV33 ( $30 \text{ fb}^{-1}$ ), which is more than the expected  $\rho_{T8}$  mass in the one-family technicolor model.

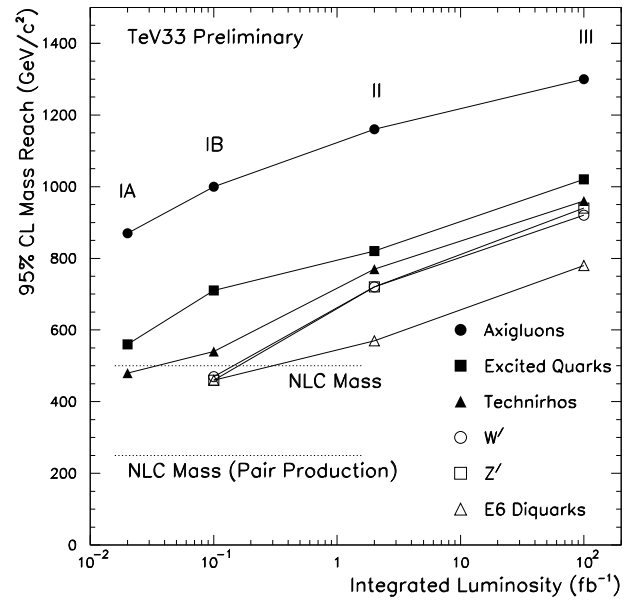


Figure 3: The mass reach for new particles decaying to dijets vs. integrated luminosity at the Tevatron. The mass reach of the NLC for direct production is also shown.

### 4. $gg \rightarrow Z_L Z_L, W_L W_L$ at LHC

Lee [6] has studied the production of longitudinal weak gauge boson pairs via gluon fusion in a one-family technicolor model [1] at the LHC. Fig. 4 shows that when the invariant mass is above the threshold for production of pairs of colored technipions, the  $W_L W_L$  or  $Z_L Z_L$  signal cross section is greater than the standard model background by over an order of magnitude. Assuming an integrated luminosity of  $100 \text{ fb}^{-1}$ , the  $Z_L Z_L$  signal, over a thousand events with four leptons in the final state (e and  $\mu$ ), will be easily observable. If one-family technicolor exists, the LHC will see it in this channel.

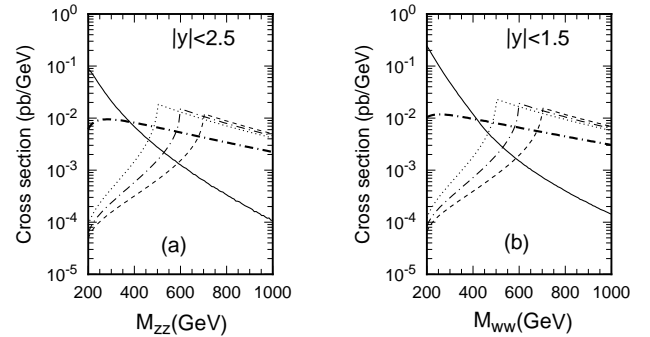


Figure 4: The cross sections for a)  $Z_L$ -pair and b)  $W_L$ -pair production via gluon fusion in proton collisions at  $E_{c.m.} = 14$  TeV. The solid curves are for the  $q\bar{q}$  initiated backgrounds, and dotted, dot-dashed, and dashed curves are for technipion masses of 250 GeV, 300 GeV, and 350 GeV respectively. The thick dot-dashed curves are for the chiral limit ( $m_{\pi_T} = 0$ ).

## B. Topcolor Assisted Technicolor

Eichten and Lane [7] have recently discussed the phenomenology of the topcolor model of Hill and Parke [8], and Burdman has recently studied the scalar sector of the model [9]. Topcolor assisted technicolor [10] is a model of dynamical electroweak symmetry breaking in which the top quark is heavy because of a new dynamics. Topcolor replaces the  $SU(3)_C$  of QCD with  $SU(3)_1$  for the third quark generation and  $SU(3)_2$  for the first two generations. The additional  $SU(3)$  symmetry produces a  $< t\bar{t} >$  condensate which makes the top quark heavy, and gives rise to a color octet gauge boson, the topgluon B. The topgluon is expected to be wide ( $\Gamma/M \approx 0.3 - 0.7$ ) and massive ( $M \sim 0.5 - 2$  TeV). In hadron collisions it is produced through a small coupling to the first two generations, and then decays via a much larger coupling to the third generation:  $q\bar{q} \rightarrow B \rightarrow b\bar{b}, t\bar{t}$ .

Similarly, topcolor also replaces  $U(1)_Y$  of the standard model with  $U(1)_{Y1}$  for the third generation and  $U(1)_{Y2}$  for the first two generations. The additional  $U(1)$  keeps the bottom quark light, and gives rise to a massive color singlet gauge boson, the topcolor  $Z'$ . The topcolor  $Z'$  may be narrow ( $\Gamma/M \sim 0.01 - 0.1$ ) and it couples predominantly to  $t\bar{t}$ .

### 1. Topgluons decaying to $b\bar{b}$ at the Tevatron

Harris [11] has used a full simulation of topgluon production and decay to  $b\bar{b}$ , and an extrapolation of the b-tagged dijet mass data [12], to estimate the topgluon discovery mass reach in a  $b\bar{b}$  resonance search. Fig. 5 displays the results for three different widths of the topgluon. The topgluon discovery mass reach,  $0.77 - 0.95$  TeV for Run II and  $1.0 - 1.2$  TeV for TeV33, covers a significant part of the expected mass range ( $\sim 0.5 - 2$  TeV).

### 2. Topgluons decaying to $t\bar{t}$ at the Tevatron

Harris [14] has used a parton level prediction for  $t\bar{t}$  production from QCD and topgluons, together with the projected experimental efficiency for reconstructing  $t\bar{t}$ , to estimate the topgluon discovery mass reach in a  $t\bar{t}$  resonance search. Fig. 6 displays the results for three different widths of the topgluon. The topgluon discovery mass reach,  $1.0 - 1.1$  TeV for Run II and  $1.3 - 1.4$  TeV for TeV33, covers a significant part of the expected mass range ( $\sim 0.5 - 2$  TeV). The mass reach estimated using the total  $t\bar{t}$  cross section, shown in Fig. 7, is similar to that for the resonance search, providing an important check. This mass reach is better than in the  $b\bar{b}$  channel, discussed in the previous section, because backgrounds in the  $t\bar{t}$  channel are smaller. If topgluons exist, there is a good chance we will find them at the Tevatron.

### 3. Topcolor $Z'$ decaying to $t\bar{t}$ at the Tevatron

Tollefson [15] has considered the decay chain topcolor  $Z' \rightarrow t\bar{t} \rightarrow (Wb)(W\bar{b}) \rightarrow l\nu b\bar{b}jj$ . She uses the PYTHIA Monte Carlo [16] and a CDF detector simulation for both the signal and background. As in the CDF top quark mass analysis [17], she requires a central charged lepton with  $E_T > 20$  GeV, a neutrino with  $E_T > 20$  GeV, 3 jets with  $E_T > 15$  GeV and  $|\eta| < 2$ , one jet with  $E_T > 8$  GeV and  $|\eta| < 2.4$  and requires

that at least two of the four jets be tagged as a  $b$  quark. She reconstructs the  $t\bar{t}$  mass with the following mass constraints: the charged lepton and neutrino reconstruct to the mass of a W, the two jets reconstruct to the mass of a W, and the mass of each reconstructed top quark be 175 GeV. This results in  $t\bar{t}$  mass resolution of 6% and an acceptance of 6.5% for the signal. From a binned maximum likelihood fit of the simulated  $t\bar{t}$  mass distribution, she determines what resonance cross section would produce a  $5\sigma$  signal, and compares that to the expected topcolor  $Z'$  cross section in Fig. 8. The resulting mass reach for a narrow topcolor  $Z'$  at the Tevatron is 0.9 TeV for Run II ( $2 \text{ fb}^{-1}$ ) and 1.1 TeV for TeV33 ( $30 \text{ fb}^{-1}$ ).

## II. COMPOSITE FERMIONS

The repetition of the three generations of quarks and leptons strongly suggests that they are composite structures made up of more fundamental fermions, which are often called “preons” in the literature. There have been a lot of theoretical efforts to construct realistic models for composite fermions, but no obviously correct or compelling model exists. Nor do we know the energy scale  $\Lambda$  which characterizes the interactions of preons.

### A. Contact Interactions

Deviations from the Standard Model (SM) in low energy phenomena can be systematically studied using the effective Lagrangian approach. In this approach, an effective Lagrangian, which obeys the low energy SM symmetries, is constructed out

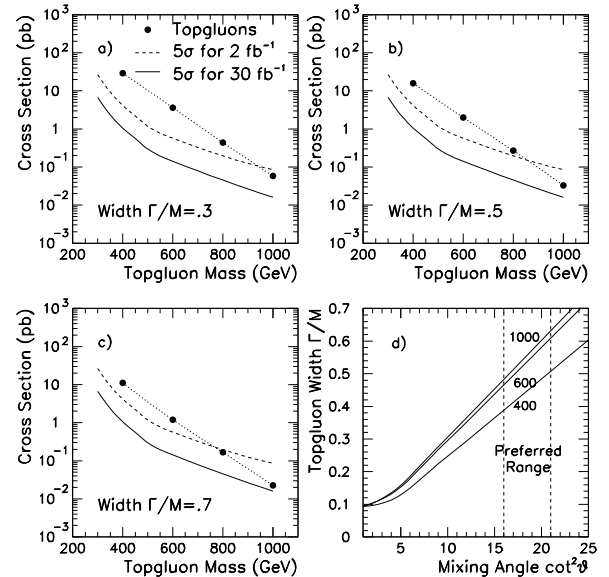


Figure 5: The mass reach for  $b\bar{b}$  decays of topgluons of width a) 0.3 M, b) 0.5 M, and c) 0.7 M. The cross section for topgluons (points) is compared to the  $5\sigma$  discovery reach of the Tevatron with a luminosity of  $2 \text{ fb}^{-1}$  (dashed) and  $30 \text{ fb}^{-1}$  (solid). d) Topgluon width as a function of mixing angle between  $SU(3)_1$  and  $SU(3)_2$  for 3 topgluon masses (curves). The vertical dashed lines are the theoretically preferred range of mixing angle [13].

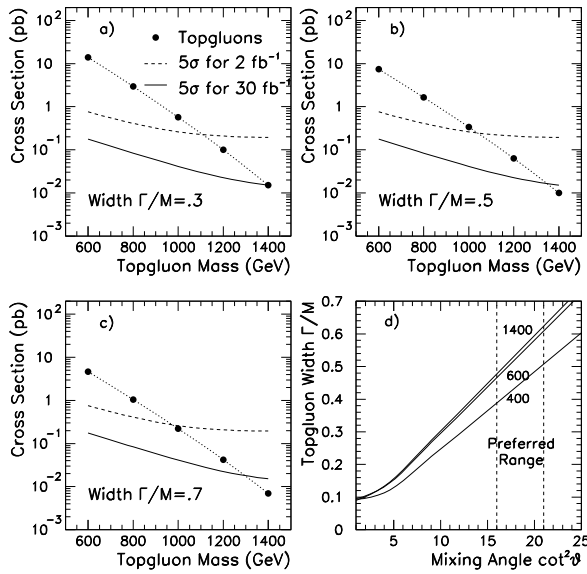


Figure 6: Same as Fig. 5 for  $t\bar{t}$  decays of topgluons.

of the SM fields. The leading terms are simply given by the SM, while the higher order terms consist of higher-dimension operators and are suppressed by powers of the scale  $\Lambda$  of the new physics.

The existence of quark and lepton substructure will be signaled by the appearance of the four-fermion contact interactions at energies below  $\Lambda$  [18]. Eichten and Lane have reviewed these contact interactions [7]. They arise from the exchanges of preon bound states, and they must be  $SU(3) \otimes SU(2) \otimes U(1)$  invariant because they are generated by forces operating at or above the electroweak scale. The lowest order four-fermion contact interactions are of dim-6, which means that they are suppressed by  $1/\Lambda^2$ . The general Lagrangian of four-fermion contact interactions, up to dimension 6, can be written as

$$\mathcal{L} \sim \frac{g^2 \eta}{2\Lambda^2} \left( \bar{q} \gamma^\mu q + \mathcal{F}_\ell \bar{\ell} \gamma^\mu \ell \right)_{L/R} \left( \bar{q} \gamma_\mu q + \mathcal{F}_\ell \bar{\ell} \gamma_\mu \ell \right)_{L/R} \quad (1)$$

where we have suppressed the generation and color indices,  $\eta = \pm 1$ , and  $\mathcal{F}_\ell$  is inserted to allow for different quark and lepton couplings but is expected to be  $\mathcal{O}(1)$ . It is conventional to define  $g^2 = 4\pi$ , so that the interaction is defined to be strong when  $\hat{s}$  approaches  $\Lambda$ . These contact interactions can affect jet production, the Drell-Yan process, lepton scattering, etc. Since compared to the SM the contact interaction amplitudes are of order  $\hat{s}/\alpha_S \Lambda^2$  or  $\hat{s}/\alpha_{em} \Lambda^2$ , the effects of the contact interactions will be most important in the phase space region with large  $\hat{s}$ . Therefore, the four-fermion contact interactions are often searched for at the high  $E_T$  region in jet and lepton-pair production. So far, the contact interaction used most to parameterize the substructure scale  $\Lambda$ , is the product of two left-handed electroweak isoscalar quark and lepton currents.

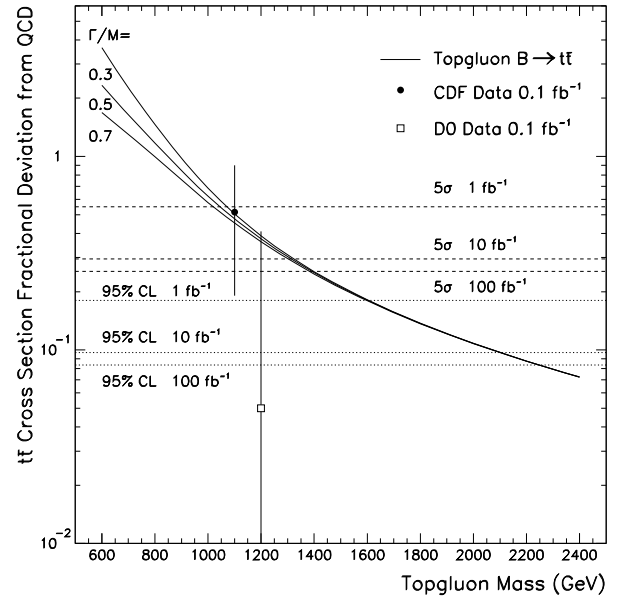


Figure 7: The fractional difference between the  $t\bar{t}$  cross section and the QCD prediction is shown for topgluons (solid curves), CDF data (solid circle), and D0 data (open box). The projected  $5\sigma$  uncertainty (dashed lines) and 95% CL (dotted lines) on the measured  $t\bar{t}$  cross section can be compared with the topgluon prediction to determine the discovery reach and exclusion reach of the Tevatron at the luminosities of 1, 10 and  $100 \text{ fb}^{-1}$ .

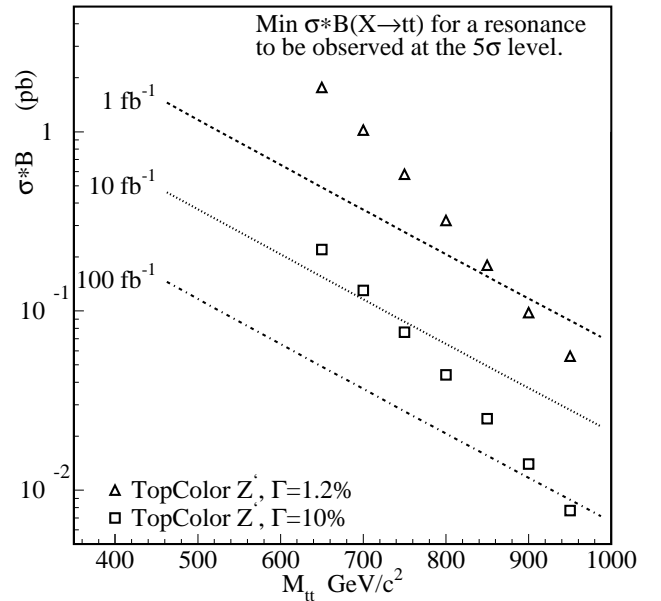


Figure 8:  $\sigma \cdot B(X \rightarrow t\bar{t})$  vs.  $t\bar{t}$  mass. The minimum cross section to observe a  $5\sigma$  excess of events in a sample with 1, 10 and  $100 \text{ fb}^{-1}$  (lines) is compared to the expected cross section for a topcolor  $Z'$  with width  $\Gamma/M = .012$  (triangles) and  $\Gamma/M = .1$  (squares).

### 1. $\bar{l}l \rightarrow q\bar{q}$ and $\bar{l}l \rightarrow l'\bar{l}'$ Contact

Table I: 95% CL lower bounds on  $\Lambda$  at lepton colliders, as a function of center of mass energy and integrated luminosity, shown for each possible helicity of the interaction.

$e^+e^-$ Colliders						
$\sqrt{s}$ TeV	$L$ $\text{fb}^{-1}$	Process	$\Lambda$ in TeV			
			$LL$	$LR$	$RL$	$RR$
0.5	50	$e^-e^+ \rightarrow \mu^+\mu^-$	19	16	16	18
		$e^-e^+ \rightarrow b\bar{b}$	24	18	5.5	16
		$e^-e^+ \rightarrow c\bar{c}$	20	4.2	5.6	17
1.0	200	$e^-e^+ \rightarrow \mu^+\mu^-$	37	33	33	36
		$e^-e^+ \rightarrow b\bar{b}$	48	36	11	33
		$e^-e^+ \rightarrow c\bar{c}$	5.1	8.3	11	5.9
1.5	200	$e^-e^+ \rightarrow \mu^+\mu^-$	45	40	40	44
		$e^-e^+ \rightarrow b\bar{b}$	59	44	17	41
		$e^-e^+ \rightarrow c\bar{c}$	7.7	12	16	8.9
5.0	1000	$e^-e^+ \rightarrow \mu^+\mu^-$	120	110	110	120
		$e^-e^+ \rightarrow b\bar{b}$	160	120	54	110
		$e^-e^+ \rightarrow c\bar{c}$	26	40	51	29

$\mu^+\mu^-$ Colliders						
0.5	0.7		6.3	5.7	5.7	6.1
		$\mu^-\mu^+ \rightarrow \tau^+\tau^-$	8.0	6.3	4.3	6.1
		$\mu^-\mu^+ \rightarrow b\bar{b}$	6.9	3.5	4.0	2.7
		$\mu^-\mu^+ \rightarrow c\bar{c}$				
0.5	50	$\mu^-\mu^+ \rightarrow \tau^+\tau^-$	19	16	16	18
		$\mu^-\mu^+ \rightarrow b\bar{b}$	24	18	5.5	16
		$\mu^-\mu^+ \rightarrow c\bar{c}$	20	4.2	5.6	17
4.0	1000	$\mu^-\mu^+ \rightarrow \tau^+\tau^-$	110	99	99	110
		$\mu^-\mu^+ \rightarrow b\bar{b}$	140	110	44	100
		$\mu^-\mu^+ \rightarrow c\bar{c}$	20	33	42	24

Cheung, Godfrey, and Hewett [19] studied the  $\ell\ell q\bar{q}$  and  $\ell\ell\ell'\bar{\ell}'$  contact interactions at future  $e^+e^-$  and  $\mu^+\mu^-$  colliders, and derived limits on the compositeness mass scale  $\Lambda$  using the reactions  $\ell^+\ell^- \rightarrow f\bar{f}$ , where  $f = \mu, \tau, b, c$  and  $\ell = e, \mu$  ( $\ell \neq f$ ). These reactions proceed via  $s$ -channel exchanges of  $\gamma$ ,  $Z$ , and the  $\ell\ell f\bar{f}$  contact interaction. The polarized differential cross sections for  $e_{L/R}^+e^- \rightarrow f\bar{f}$  versus  $\cos\theta$ , where  $\theta$  is the scattering angle in the CM frame, are given by

$$\frac{d\sigma_L}{d\cos\theta} = \frac{\pi\alpha^2 C_f}{4s} \{ |C_{LL}|^2 (1 + \cos\theta)^2 + |C_{LR}|^2 (1 - \cos\theta)^2 \} \quad (2)$$

where

$$C_{LL} = -Q_f + \frac{C_L^e C_L^f}{c_w^2 s_w^2} \frac{s}{s - M_Z^2 + i\Gamma_Z M_Z} + \frac{s\eta_{LL}}{2\alpha\Lambda^2} \quad (3)$$

$$C_{LR} = -Q_f + \frac{C_L^e C_R^f}{c_w^2 s_w^2} \frac{s}{s - M_Z^2 + i\Gamma_Z M_Z} + \frac{s\eta_{LR}}{2\alpha\Lambda^2} \quad (4)$$

and  $C_L^f = T_{3f} - Q_f s_w^2$ ,  $C_R^f = -Q_f s_w^2$ ,  $C_f = 3(1)$  for  $f$  being a quark (lepton),  $s_w$  and  $c_w$  are, respectively, the sine and cosine of the weak mixing angle. The expressions for  $d\sigma_R/d\cos\theta$ ,  $C_{RR}$ , and  $C_{RL}$  can be obtained by interchanging  $L \leftrightarrow R$ . The unpolarized differential cross section is simply given by the average of  $d\sigma_L/d\cos\theta$  and  $d\sigma_R/d\cos\theta$ . Other observables, e.g.,  $A_{FB}$ ,  $A_{LR}$ , can be obtained from these  $\cos\theta$  distributions.

To obtain the sensitivity to the compositeness scale they assume that the SM is correct and perform a  $\chi^2$  analysis of the  $\cos\theta$  distribution for the theory with a finite  $\Lambda$ . An acceptance cut  $|\cos\theta| < 0.9$  was imposed and the whole  $\cos\theta$  distribution is divided into 10 equal bins. The efficiencies in detecting the final state are  $\epsilon = 60\%$  for  $b$  quarks, 35% for  $c$  quarks, and 100% for leptons. The limits on  $\Lambda$  at 95% CL that can be obtained by various processes at future  $e^+e^-$  and  $\mu^+\mu^-$  colliders are tabulated in Table I. Very substantial improvements in probing the compositeness mass scale can be achieved. A 0.5 TeV  $e^+e^-$  collider with a 50  $\text{fb}^{-1}$  luminosity can probe up to around 20 TeV, which is better than Run II of the Tevatron. Up to about 40, 60, and 160 TeV can be probed at  $\sqrt{s} = 1.0, 1.5$ , and 5.0 TeV  $e^+e^-$  machines, respectively. A 4 TeV  $\mu^+\mu^-$  collider, which is under intensive study, can probe up to about 140 TeV. Slightly better results can be obtained by using polarized  $e^-$  beams with the same luminosity [19].

### 2. $q\bar{q} \rightarrow \bar{l}l$ Contact

P. de Barbaro *et al* [20] have studied the effect of a left-handed contact interaction between quarks and leptons at the Tevatron. Using 110  $\text{pb}^{-1}$  of CDF data on dielectron production, they report preliminary limits of  $\Lambda_{LL}^-(q\bar{q} \rightarrow e^+e^-) \geq 3.4$  TeV and  $\Lambda_{LL}^+(q\bar{q} \rightarrow e^+e^-) \geq 2.4$  TeV at 95% CL. They also report limits for the dimuon channel and the combined dielectron+dimuon channels; the latter is approximately 0.5 TeV more stringent than with electrons alone. Using a Monte Carlo procedure they estimate the sensitivity of the Tevatron with higher luminosities.

For standard model production of dielectrons they simulate one hundred experiments with 2  $\text{fb}^{-1}$  and one hundred experiments with 30  $\text{fb}^{-1}$ , each measuring the dielectron mass spectrum. For each experiment they calculate a likelihood as a function of  $\Lambda$  of that experiment coming from the standard model plus a contact interaction of strength  $\Lambda$ . To minimize fluctuations in the shape of the likelihood function, they average the likelihood functions from the 100 experiments. In Figure 9 they plot the log likelihood as a function of  $\eta/\Lambda$ , where  $\eta$  is the sign of the contact interaction. From Fig. 9 a Tevatron experiment with 2  $\text{fb}^{-1}$  would exclude  $\Lambda_{LL}^-(q\bar{q} \rightarrow e^+e^-) \leq 10$  TeV and  $\Lambda_{LL}^+(q\bar{q} \rightarrow e^+e^-) \leq 6.5$  TeV, and 30  $\text{fb}^{-1}$  would exclude  $\Lambda_{LL}^-(q\bar{q} \rightarrow e^+e^-) \leq 20$  TeV and  $\Lambda_{LL}^+(q\bar{q} \rightarrow e^+e^-) \leq 14$  TeV. The sensitivity is always greater for  $\eta = -1$ , because this corresponds to constructive interference between the standard model and the contact interaction, and hence a larger number of dielectrons.

### 3. $q\bar{q} \rightarrow q\bar{q}$ Contact

An excess of events with high jet  $E_T$  in hadron collisions is a well known signature for a  $q\bar{q} \rightarrow q\bar{q}$  contact interaction. However, significant uncertainties in the parton momentum distributions within the proton, ambiguities in QCD calculations, and systematic uncertainties in jet energy measurement, make it difficult to discover a signal. This is apparent from the recent CDF measurement of the inclusive jet cross section [21], and the phenomenological papers which followed [22]. Some progress has been made at the Snowmass workshop on quantifying the un-

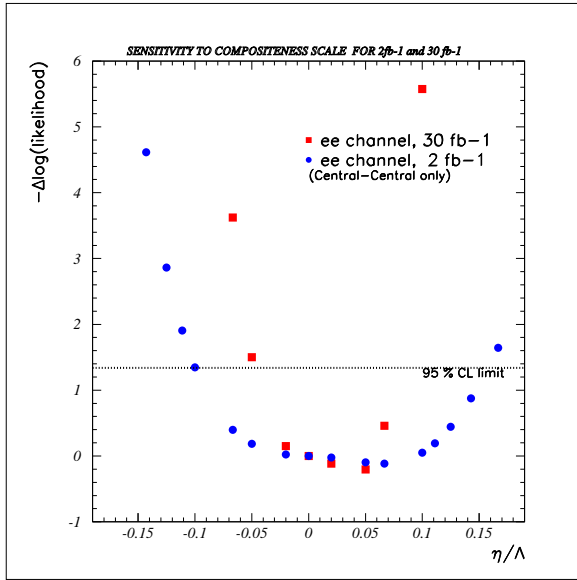


Figure 9: The change in the log likelihood function from the maximum plotted as a function of  $\eta \times 1/\Lambda$  for  $ee$  channel with  $2 \text{ fb}^{-1}$  (circles) and  $30 \text{ fb}^{-1}$  (squares). The 95% CL one sided limit occurs where the solid line at 1.34 intersects the points.

certainties in the parton distributions [23], however, more work is clearly necessary. Another signal of a  $q\bar{q} \rightarrow q\bar{q}$  contact interaction, which is not very sensitive to theoretical or jet energy measurement, is a dijet angular distribution which is more isotropic than predicted by QCD. Using  $110 \text{ pb}^{-1}$  of data at the Tevatron, CDF has recently measured the dijet angular distribution and found good agreement with QCD predictions, thereby excluding a contact interaction among up and down type quarks with scale  $\Lambda^+ \leq 1.6 \text{ TeV}$  or  $\Lambda^- \leq 1.4 \text{ TeV}$  at 95% CL [24]. For a flavor symmetric contact interaction among all quarks the exclusions are 0.2 TeV more. Although with further luminosity this exclusion will improve somewhat, comparing this limit with that obtained from the UA1 experiment [25], we see that the compositeness scale reach of a hadron collider is roughly equal to its center of mass energy,  $\sqrt{s}$ . This is confirmed by studies of the LHC [26], where the predicted reach is  $\Lambda \approx 15 \text{ TeV}$ .

#### 4. $q\bar{q} \rightarrow \gamma\gamma$ Contact Interaction

Rizzo has previously studied the effects of a  $q\bar{q} \rightarrow \gamma\gamma$  contact interaction at the Tevatron and the LHC [27] and here he extends these results to a Very Large Hadron Collider (VLHC) [28]. The lowest dimension gauge invariant operator involving two fermions and two photons is a dimension-8 operator, which induces a  $q\bar{q}\gamma\gamma$  contact interaction. This interaction, assuming parity and CP conservation, is given by

$$\mathcal{L} = \frac{2ie^2}{\Lambda^4} Q_q^2 F^{\mu\sigma} F_\sigma^\nu \bar{q}\gamma_\mu \partial_\nu q, \quad (5)$$

where  $e$  is the electromagnetic coupling, and  $\Lambda$  is the associated mass scale. The observation of the signatures associated

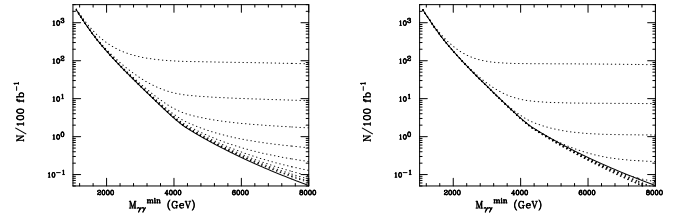


Figure 10: Event rate for isolated  $\gamma\gamma$  events with invariant masses larger than  $M_{\gamma\gamma}^{\min}$  at a 60 TeV  $pp$  collider scaled to a luminosity of  $100 \text{ fb}^{-1}$ . The solid curves is the SM case while the top dotted curve corresponds to  $\Lambda_+(\Lambda_-) = 3 \text{ TeV}$  in the left (right) figure. Each subsequent dotted curve corresponds to an increase in  $\Lambda_\pm$  by 1 TeV. In either case we have applied the cuts  $p_t^\gamma \geq 500 \text{ GeV}$  and  $|\eta_\gamma| \leq 1$ .

with this operator would be a clear signal of compositeness. The mass scale  $\Lambda^\pm$  indicates that the limits obtained below will depend upon whether the contact operator interferes constructively or destructively with the SM contribution. It is clear that the contact interaction in (5) affects the parton cross section most in the region with large  $\hat{s}$ , and thus it causes the cross section to be less peaked in the forward and backward directions and generates more central and higher  $p_T$  photons. It also enhances the production rate at high diphoton invariant mass  $M_{\gamma\gamma}$ .

Figure 10 shows the integrated event rates for isolated diphoton events with invariant mass larger than  $M_{\gamma\gamma}^{\min}$  at a 60 TeV  $pp$  collider with a  $100 \text{ fb}^{-1}$  luminosity. It clearly shows that the contact interaction of Eq.(5) changes the cross sections most in the high  $M_{\gamma\gamma}^{\min}$  region. In order to obtain the sensitivity to the contact interaction, we can assume that there is no event excess over the SM predictions in various future collider experiments, and then we can put limits on  $\Lambda^\pm$  using a simple  $\chi^2$  analysis. The results for various future collider experiments are tabulated in Table II. From the table we can see that  $p\bar{p}$  colliders are better than  $pp$  colliders because there are more  $q\bar{q}$  luminosities in  $p\bar{p}$  than in  $pp$ . The limits can be pushed to about 7–13 TeV at a 60 TeV machine, and about 16–33 TeV at a 200 TeV one.

Table II: 95% CL bounds on the scale of the  $q\bar{q}\gamma\gamma$  contact interaction at future hadron colliders. Here,  $p_t^{\min}$  is the minimum transverse momentum of each of the photons in GeV,  $\mathcal{L}$  is the machine integrated luminosity in  $\text{fb}^{-1}$ , and  $\Lambda^\pm$  is the lower bound on the scale in TeV.

Machine	$p_t^{\min}$	$ \eta_{\gamma, \max} $	$\mathcal{L}$	$\Lambda^+$	$\Lambda^-$
TeV	15	1	2	0.75	0.71
LHC	200	1,2,5	100	2.8	2.9
60 TeV ( $pp$ )	500	1	100	$\simeq 9.5$	$\simeq 6.5$
60 TeV ( $p\bar{p}$ )	500	1	100	$\simeq 13.5$	$\simeq 10.5$
200 TeV ( $pp$ )	1000	1	1000	$\simeq 23$	$\simeq 16$
200 TeV ( $p\bar{p}$ )	1000	1	1000	$\simeq 33$	$\simeq 26$

## B. Excited Quarks

Although it is expected that the first evidence for quark and/or lepton substructure would arise from the affects of contact interactions, conclusive evidence would be provided by observation of excitations of the preon bound state. If quarks are composite particles then excited quarks are expected. Harris [29] has investigated the prospects for discovering an excited quark [30],  $u^*$  or  $d^*$  with spin 1/2 and weak isospin 1/2, at hadron colliders. He considers the process  $qg \rightarrow q^* \rightarrow qg$ , and does a lowest order calculation of the dijet resonance signal and QCD background assuming an experimental dijet mass resolution of 10%. The estimated  $5\sigma$  discovery mass reach at the Tevatron is 0.94 TeV for Run II ( $2 \text{ fb}^{-1}$ ) and 1.1 TeV for TeV33 ( $30 \text{ fb}^{-1}$ ). The mass reach at the LHC is 6.3 TeV for  $100 \text{ fb}^{-1}$ . The discovery mass reach at a Very Large Hadron Collider (VLHC) is shown in Fig. 11 for 3 different machine energies as a function of integrated luminosity. At a VLHC with a center of mass energy of (50) 200 TeV the mass reach is 25 TeV (78 TeV) for an integrated luminosity of  $10^4 \text{ fb}^{-1}$ . However, an excited quark with a mass of 25 TeV would be discovered at a hadron collider with  $\sqrt{s} = 100 \text{ TeV}$  and an integrated luminosity of only  $13 \text{ fb}^{-1}$ ; here a factor of 2 increase in energy from a 50 TeV to a 100 TeV machine is worth a factor of 1000 increase in luminosity at a fixed machine energy of 50 TeV.

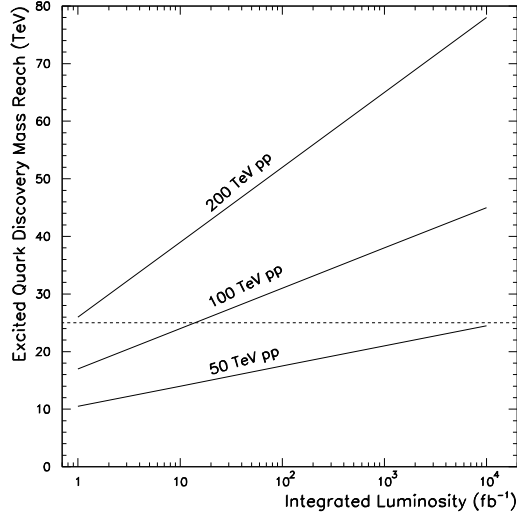


Figure 11: The  $5\sigma$  discovery mass reach, for excited quarks decaying to dijets, is shown as a function of integrated luminosity for a VLHC with  $\sqrt{s} = 50 \text{ TeV}$ ,  $100 \text{ TeV}$  and  $200 \text{ TeV}$  (solid curves). The horizontal dashed line demonstrates what luminosity is necessary to discover a 25 TeV excited quark.

## III. ANOMALOUS COUPLINGS OF QUARKS

The lowest order interaction between a quark and a gluon is a dimension-4 operator,  $\bar{t}\gamma^\mu T_a t G_\mu^a$ . Among all the dimension-5 operators, the most interesting ones involving quarks and gluons are the chromomagnetic (CMDM) and chromoelectric (CEDM) dipole moment couplings of quarks. These dipole moment couplings are important not only because they are only suppressed by one power of  $\Lambda$  but also because a nonzero value for the

CEDM is a clean signal for CP violation. The effects of these anomalous couplings have been studied quite extensively, e.g., in  $t\bar{t}$  production [31, 32, 33], in  $b\bar{b}$  production [31], and in inclusive jet production [34].

The effective Lagrangian for the interactions between a quark and a gluon that include the CEDM and CMDM form factors is

$$\mathcal{L}_{\text{eff}} = g_s \bar{q} T^a \left[ -\gamma^\mu G_\mu^a + \frac{\kappa}{4m_q} \sigma^{\mu\nu} G_{\mu\nu}^a - \frac{i\tilde{\kappa}}{4m_q} \sigma^{\mu\nu} \gamma^5 G_{\mu\nu}^a \right] q. \quad (6)$$

where  $\kappa/2m_q$  ( $\tilde{\kappa}/2m_q$ ) is the CMDM (CEDM) of the quark  $q$ . The above Lagrangian is valid for both light and heavy quarks. The Lagrangian in Eq. (6) gives an effective  $qqg$  vertex, and also induces a  $qqgg$  interaction, which is absent in the SM. We shall use a short-hand notation:

$$\kappa' = \frac{\kappa}{2m_q}, \quad \tilde{\kappa}' = \frac{\tilde{\kappa}}{2m_q} \quad (7)$$

which are given in units of  $(\text{GeV})^{-1}$ .

### A. Prompt Photon Production

Cheung and Silverman have studied the effects of anomalous CMDM and CEDM of light quarks on prompt photon production [35]. Prompt photon production is sensitive to the gluon luminosity inside a hadron because it is mainly produced by quark-gluon scattering. For the same reason this process is also sensitive to the anomalous couplings of quarks to gluons. The contributing subprocesses for prompt photon production are:  $q(\bar{q})g \rightarrow \gamma q(\bar{q})$  and  $q\bar{q} \rightarrow \gamma g$ . The spin- and color-averaged amplitude for  $q(p_1)g(p_2) \rightarrow \gamma(k_1)q(k_2)$  is given by

$$\overline{\sum} |\mathcal{M}|^2 = \frac{16\pi^2 \alpha_s \alpha_{\text{em}} Q_q^2}{3} \left[ -\frac{s^2 + t^2}{st} - 2u(\kappa'^2 + \tilde{\kappa}'^2) \right] \quad (8)$$

where

$$s = (p_1 + p_2)^2, \quad t = (p_1 - k_1)^2, \quad u = (p_1 - k_2)^2, \quad (9)$$

and  $Q_q$  is the electric charge of the quark  $q$  in units of proton charge. Similarly, the spin- and color-averaged amplitude for  $q(p_1)\bar{q}(p_2) \rightarrow \gamma(k_1)g(k_2)$  is given by

$$\overline{\sum} |\mathcal{M}|^2 = \frac{128\pi^2 \alpha_s \alpha_{\text{em}} Q_q^2}{9} \left[ \frac{t^2 + u^2}{ut} + 2s(\kappa'^2 + \tilde{\kappa}'^2) \right]. \quad (10)$$

The differential cross section for prompt photon production versus the transverse momentum of the photon is shown in Fig. 12a. The LO QCD curve has to be multiplied by a  $K$ -factor of about 1.3 to best fit the CDF data. Figure 12a also shows curves with nonzero values of CMDM. It is clear that nonzero  $\kappa'$  will increase the total and the differential cross sections, especially in the large  $p_T(\gamma)$  region. The effects due to nonzero CEDM will be the same because the increase in cross section is proportional to  $(\kappa'^2 + \tilde{\kappa}'^2)$ .

The fractional difference from pure QCD for nonzero CMDM is shown in Fig. 12b. The data are from CDF [36] and D0 [37]. The anomalous behavior at low  $p_T(\gamma)$  has already been resolved by including initial and final state shower radiation, therefore,

only the large  $p_T$  region is relevant. Since in Eqs. (8) and (10) the role of  $\kappa'$  and  $\tilde{\kappa}'$  are the same, one of them is kept zero when bounding on the other. From these curves it is clear that the CDF and D0 data would be inconsistent with  $\kappa' > 0.0045$ , therefore, giving a bound of

$$\kappa' \leq 0.0045 \text{ GeV}^{-1} \quad (11)$$

on the CMDM of light quarks. Similarly, a bound of  $\tilde{\kappa}' \leq 0.0045 \text{ GeV}^{-1}$  on the CEDM of light quarks is valid as well. We compare this with the results obtained in Ref.[34] for jet production. The value of  $\kappa'$  obtained in fitting to the CDF[21] transverse energy distribution of the inclusive jet production is [34]  $\kappa' = (1.0 \pm 0.3) \times 10^{-3} \text{ GeV}^{-1}$  which is consistent with the bound in Eq. (11)

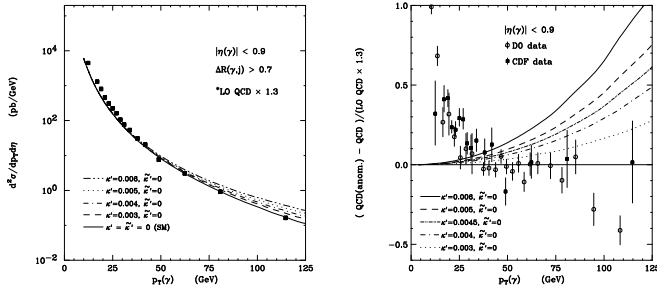


Figure 12: (a) Transverse momentum distribution  $d^2\sigma/p_T d\eta$  in prompt photon production for pure QCD and nonzero values of  $\kappa'$ . The data points are from CDF; (b) fractional difference from QCD for various values of  $\kappa'$  and  $\tilde{\kappa}'$ . Both D0 and CDF data are shown.

## B. Sensitivities in Future Collider Experiments

Silverman and Cheung [38] have estimated the sensitivity of the Tevatron and LHC to the anomalous chromomagnetic dipole moment of light quarks. A lowest order parton level calculation was used, and only the statistical sensitivity of the experiments was considered. The criterion, in the spirit of reference [26], is to take bins of appropriate size for the energy range being examined, and find the  $E_T$  called  $E_T^*$  at which the QCD cross section statistical error bars are 10%. These will be bins with 100 QCD events. Then the cross section due to QCD plus the anomalous chromomagnetic moment contribution will be explored, and the value of  $\kappa' \equiv 1/\Lambda$  or  $\Lambda$  is determined where the excess over QCD is 10% at this  $E_T^*$ . These  $E_T^*$  and  $\Lambda$  are shown in Table III. Varying the bin size by a factor of two makes only a small change in the value of  $E_T^*$  or  $\Lambda$ . The limits in  $|\eta|$  used are 0.9 for the Tevatron, and 1.0 for the LHC. From table III one can see that  $\Lambda$  sensitivity scales roughly as the beam energy.

## C. Effects on $t\bar{t}$ Production at the LHC

Top quark production at hadronic colliders is the most obvious place to probe the anomalous coupling of top quarks to gluons. There have been quite a few studies [31, 32, 33] on this subject at the Tevatron energies. Rizzo has extended the study to the LHC [39]. The contributing subprocesses to top pair production are  $q\bar{q}, gg \rightarrow t\bar{t}$ . The existence of a nonzero

Table III: Table of High  $E_T$  Bins at 10% Statistical Error and 1- $\sigma$  Sensitivity for  $\Lambda$  in that Bin, is shown as a function of machine energy, integrated luminosity, and bin width.

$E_{cm}$	Int. Lum.	Bin Width	$E_T$ Jets		Photons	
			$E_T^*$	$\Lambda$	$E_T^*$	$\Lambda$
TeV	$\text{fb}^{-1}$	GeV	GeV	TeV	GeV	TeV
1.8	0.1	10	360	1.8	140	0.7
2.0	2	20	490	2.8	260	1.5
2.0	10	20	540	3.3	325	1.9
2.0	30	20	575	3.5	370	2.1
14	10	100	2500	13	1000	4.5
14	100	100	3100	17	1400	6.3

chromomagnetic dipole moment of the top quark will change both the total and differential cross sections. Since higher partonic center-of-mass energies become accessible at the LHC, one can probe beyond the top pair production threshold region, and have much higher sensitivities to the CMDM.

Figures 13a and 13c show the modifications in the SM expectations for both  $d\sigma/dM_{t\bar{t}}$  and  $d\sigma/dp_t$ , respectively, for different values of  $\kappa$  of the top quark. Perhaps more revealing, Figures 13b and 13d show the ratio of the modified distributions to the corresponding SM ones. One can see that a non-zero  $\kappa$  leads to (i) enhanced cross sections at large  $p_t$  and  $M_{t\bar{t}}$ , and (ii) the shapes of the distributions are altered, *i.e.*, the effect is not just an overall change in normalization. The sensitivities of these distributions to nonzero  $\kappa$  are also estimated using a Monte Carlo approach, taking into account a reasonable size of systematic errors. Assuming the SM is the correct theory, the 95% CL allowed regions of  $\kappa$  of the top quark are  $-0.09 \leq \kappa \leq 0.10$  from the  $M_{t\bar{t}}$  distribution and  $0.06 \leq \kappa \leq 0.06$  from the  $p_T$  distribution.



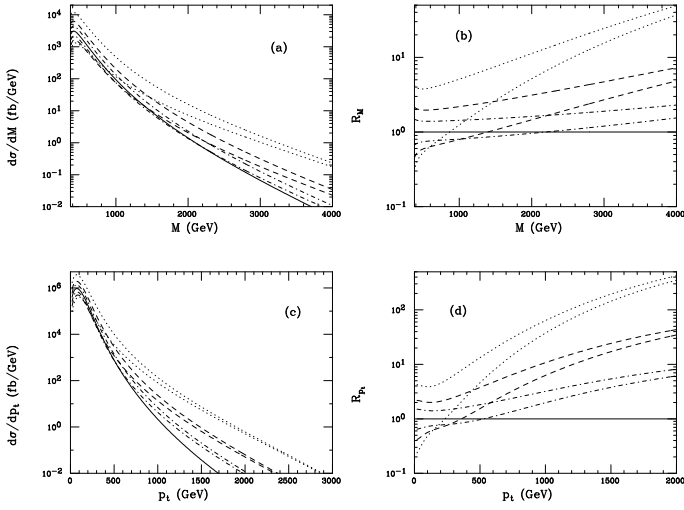


Figure 13: (a)  $t\bar{t}$  invariant mass distribution at the LHC for various values of  $\kappa$  assuming  $m_t = 180$  GeV. (b) The same distribution scaled to the SM result. (c)  $t\bar{t}$   $p_t$  distribution at the LHC and (d) the same distribution scaled to the SM. In all cases, the SM is represented by the solid curve whereas the upper(lower) pairs of dotted, dashed, and dash-dotted curves corresponds to  $\kappa = 0.5(-0.5)$ ,  $0.25(-0.25)$ , and  $0.125(-0.125)$ , respectively.

Table IV: The mass reach and discovery potential, for particles from one-family technicolor or topcolor, at the Tevatron as a function of integrated luminosity

Channel	Run I (.1 fb <sup>-1</sup> )	Run II (2 fb <sup>-1</sup> )	TeV33 (30 fb <sup>-1</sup> )
$\rho_{T1} \rightarrow W + \text{dijet}$ (no b-tagging)	No Mass Reach	No Mass Reach	$\approx 400$ GeV at 95% CL
$\rho_{T1} \rightarrow W + \text{dijet}$ (with b-tagging)	?	Discovery for $M_\rho = 210$ $M_\pi = 115$ GeV	Better than no b-tag
$\rho_{T8} \rightarrow \text{dijet}$	$0.25 < M_\rho < 0.50$ TeV at 95% CL	0.77 TeV at 95% CL	0.90 TeV at 95% CL
Topgluon $B' \rightarrow bb$ ( $0.3 < \Gamma/M < 0.7$ )	Search in Progress	0.77 – 0.95 TeV at $5\sigma$	1.0 – 1.2 TeV at $5\sigma$
Topgluon $B' \rightarrow t\bar{t}$ ( $0.3 < \Gamma/M < 0.7$ )	Search in Progress	0.97 – 1.11 TeV at $5\sigma$	1.3 – 1.4 TeV at $5\sigma$
TopC $Z' \rightarrow t\bar{t}$ ( $\Gamma/M = .012$ )	Search in Progress	920 GeV at $5\sigma$	1150 GeV at $5\sigma$

Table V: Mass and energy reach in TeV for new interactions at colliders. The symbol “ $\sim$ ” indicates a guess based on scaling from lower energy machines. “Found” indicates the collider will discover the particle if it exists, and “Already Found” indicates the particle would have already been discovered by a earlier collider. The symbol “–” means not applicable, and “?” means we don’t know. The numbers in square brackets are either confidence levels in % or RMS deviations in units of  $\sigma$ , indicating the statistical size of the effect corresponding to the mass or energy reach.

Particle or Interaction Scale	Collider				
	TeV33 2 TeV, $p\bar{p}$ 30 $fb^{-1}$	LHC 14 TeV, $pp$ 100 $fb^{-1}$	VLHC 200 TeV, $pp$ 1000 $fb^{-1}$	NLC .5 TeV, $e^+e^-$ 50 $fb^{-1}$	Muon 4 TeV, $\mu^+\mu^-$ 1000 $fb^{-1}$
Technicolor $\rho_{T1}$	.4 [95%]	$> 1^*$	?	$1.5^\dagger$ [6.7 $\sigma$ ]	$\sim 10$
Techni $\rho_{T8} \rightarrow \text{dijet}$	Found	Already Found			
Topcolor $Z' \rightarrow t\bar{t}$	1.1 [5 $\sigma$ ]	Found	Already Found		
Topgluon $B \rightarrow b\bar{b}, t\bar{t}$	1.4 [5 $\sigma$ ]	Found	Already Found		
$\Lambda_{LL}(l\bar{l} \rightarrow l'\bar{l}')$	–	–	–	19 [95%]	110 [95%]
$\Lambda_{LL}(qq \rightarrow qq)$	2	15*	$\sim 200$	–	–
$\Lambda_{LL}(q\bar{q} \leftrightarrow l\bar{l})$	20 [95%]	$\sim 100$	$\sim 1000$	24 [95%]	140 [95%]
$\Lambda(q\bar{q} \rightarrow \gamma\gamma)$	0.9 [95%]	3 [95%]	20 [95%]	–	–
Excited Quark	1.1 [5 $\sigma$ ]	6.3 [5 $\sigma$ ]	78 [5 $\sigma$ ]	$0.45^\dagger$	$\sim 3$
CMDM $\Lambda$ (dijets)	3.5 [ $> 1\sigma$ ]	17 [ $> 1\sigma$ ]	?	–	–
CMDM $\Lambda$ ( $\gamma$ +jet)	2.1 [ $> 1\sigma$ ]	6.3 [ $> 1\sigma$ ]	?	–	–

\* from reference [26]     $^\dagger$  from reference [40]

## D. Summary and Conclusions

Table IV and V summarize the ability of colliders to answer fundamental questions involving new interactions.

Is electroweak symmetry broken by the dynamics of a new interaction? We see that a color singlet technirho can be discovered at the Tevatron if it has the mass expected within the one-family technicolor model. Simpler models of technicolor, where there are only color singlet techniquarks and no technileptons, would predict technirho masses of a TeV or more. These could be discovered at the LHC or NLC, and higher mass technirhos could be observed at a VLHC or a muon collider. Color octet technirhos can be discovered at the Tevatron if they have the mass expected within the one-family technicolor model.

Is the mass difference between the top quark and the other quarks generated by a new interaction? Topcolor assisted technicolor can be discovered at the Tevatron if the topgluon or topcolor  $Z'$  has mass around a TeV or less, which is possible. The topgluon and topcolor  $Z'$  are expected to be lighter than a few TeV, so if they are missed by the Tevatron they will be discovered by the LHC.

Are quarks and leptons composite particles held together by new interactions? If the energy scale of those interactions is less than 20 TeV, the Tevatron has a chance of discovery in the dilepton mass spectrum, the NLC has a slightly better chance of discovery using dijet angular distributions, and the LHC will certainly see this scale of  $q\bar{q} \leftrightarrow l\bar{l}$  contact interaction. Proof that observed contact interactions were caused by compositeness would come from the observation of excited states with mass near the compositeness scale. To discover an excited quark with mass around 20 TeV, we would have to build a VLHC colliding protons with  $\sqrt{s} = 50 - 200$  TeV.

Is there a new interaction which changes the coupling of quarks and gluons at high energies? The Tevatron can probe anomalous coupling energy scales of a few TeV, and the LHC can probe 17 TeV for light quarks and is sensitive to top quark anomalous couplings.

We conclude that there is a significant chance of discovering new interactions at the Tevatron in the next decade. From Table V the reader can determine which of the proposed future colliders provide the greatest additional discovery potential in the post-Tevatron era.

## IV. REFERENCES

- [1] E. Eichten and K. Lane, Fermilab-Conf-96/297-T, BUHEP-96-33, hep-ph/9609297, and these proceedings.
- [2] D. Toback, Fermilab-Conf-96/360 and these proceedings.
- [3] J. Womersley, these proceedings.
- [4] F. Abe *et al.* (CDF Collaboration), Phys. Rev. Lett. **74**, 3538 (1995).
- [5] D. Amidei and R. Brock, *Report of the TeV2000 Study Group*, Fermilab-Pub-96/082.
- [6] T. Lee, these proceedings.
- [7] E. Eichten and K. Lane, Fermilab-Conf-96/298-T, BUHEP-96-34, hep-ph/9609298, and these proceedings.
- [8] C. Hill and S. Parke, Phys. Rev. **D49**, 4454 (1994).
- [9] G. Burdman, these proceedings.
- [10] C. Hill, Phys. Lett. **B345**, 483 (1995).
- [11] R. Harris, Fermilab-Conf-96/276-E, hep-ph/9609316, and these proceedings.
- [12] R. Harris (CDF Collaboration), hep-ex/9506008, Fermilab-conf-95/152-E.
- [13] G. Buchalla, G. Burdman, C. Hill and D. Kominis, Phys. Rev. **D53**, 5185 (1996).
- [14] R. Harris, Fermilab-Conf-96/277-E, hep-ph/9609318, and these proceedings.
- [15] K. Tollefson in reference [5].
- [16] T. Sjostrand, computer code PYTHIA V5.6, CERN-TH-6488/92.
- [17] F. Abe *et al.* (CDF Collaboration), Phys. Rev. Lett. **74**, 2626 (1995).
- [18] E. Eichten, K. Lane, and M. Peskin, Phys. Rev. Lett. **50**, 811 (1983).
- [19] K. Cheung, S. Godfrey, and J. Hewett, these proceedings.
- [20] P. de Barbaro *et al.*, Fermilab-Conf-96/356-E, and these proceedings.
- [21] F. Abe *et al.* (CDF Collaboration), Phys. Rev. Lett. **77**, 438 (1996).
- [22] J. Huston *et al.*, Phys. Rev. Lett. **77**, 444 (1996); H. L. Lai *et al.*, MSU-HEP-60426, hep-ph/9606399 (1996), submitted to Phys. Rev. D.
- [23] F. Olness, these proceedings.
- [24] F. Abe *et al.* (CDF Collaboration), Fermilab-Pub-96/317-E, hep-ex/9609011, submitted to Phys. Rev. Lett.
- [25] G. Arnison, *et al.*, Phys. Lett. **B177**, 244(1986)
- [26] U.S. ATLAS and U.S. CMS Coll., edited by I. Hinchliffe and J. Womersley, LBNL-38997 (1996).
- [27] T. Rizzo, Phys. Rev. **D51**, 1064 (1994).
- [28] *Constraint on  $q\bar{q}\gamma\gamma$  Contact Interactions at Future Hadron Colliders*, T. Rizzo, in these proceedings.
- [29] R. Harris, Fermilab-Conf-96/285-E, hep-ph/9609319, and these proceedings.
- [30] U. Baur, I. Hinchliffe and D. Zeppenfeld, Int. J. of Mod. Phys. **A2**, 1285 (1987) and U. Baur, M. Spira and P. M. Zerwas, Phys. Rev. **D42**, 815 (1990).
- [31] D. Atwood, A. Kagan, and T. Rizzo, Phys. Rev. **D52**, 6254 (1995).
- [32] P. Haberl, O. Nachtmann, and A. Wilch, Phys. Rev. **D53**, 4875 (1996).
- [33] K. Cheung, Phys. Rev. **D53**, 3604 (1996).
- [34] D. Silverman, hep-ph/9605318, to be published in Phys. Rev. **D**.
- [35] *Limits on Anomalous Couplings of Quarks by Prompt Photon Data*, K. Cheung and D. Silverman, in these proceedings.
- [36] F. Abe *et al.* (CDF Collaboration), Phys. Rev. Lett. **73**, 2662 (1994).
- [37] S. Abachi *et al.* (D0 Collaboration), FERMILAB-PUB-96/072-E.
- [38] *Quark Anomalous Chromomagnetic Moment Bounds - Projection to Higher Luminosities and Energy*, K. Cheung and D. Silverman, in these proceedings.
- [39] *Constraints on Anomalous Top Quark Couplings at the LHC*, T. Rizzo, in these proceedings.
- [40] The NLC ZDR, Fermilab-Pub-96/112.